Rev. Roum. Sci. Techn.– Électrotechn. et Énerg.
Vol. **67**, *1*, pp. 81–86, Bucarest, 2022

Thermotechnique et thermoénergétique

FLOW AND HEAT TRANSFER IN AN AGING HEAT FURNACE FOR ALUMINUM ALLOY PLATES

ALEXANDRU M. MOREGA[1], MARIN PETRE[2], YELDA VELI[1], ALIN A. DOBRE[1]

Key words: Aging heat treatment, Heat furnace, Aluminum alloy plates, Numerical simulation, Finite element method.

Structural materials for the aerospace industry require high hardness and easy machining in certain tempers that, particularly, 2014 aluminum alloy may withstand successfully. The proper aging heat treatment from the aluminum raw plate, from the initial, hall temperature, all the way to the final product, which may take up to roughly 9 hours, is an important quality concern. An important role in understanding these thermal processes is played by mathematical modeling, which provides for the ability to simulate and optimize such processes at an industrial scale. Numerical modeling is used here to assist the optimization of the aging process. The results compare well with the available industrial tests data on an indirectly heated, fuel-fired batch furnace that is used to this end. This study is aimed to model the airflow inside the furnace during the aging process with a particular focus on predicting the dynamics of the internal thermal field distribution.

1. INTRODUCTION

In the process of making aluminum sheets heat treatments play an essential role. After age hardening through solution heat treatment and quenching precipitation, the Al alloys (including 2000, 6000, and 7000 series) undergo aging by heating. The natural aging heat treatment can be produced at room temperature, for several days, while artificial aging requires elevated temperatures, usually in the range of 150 to 200 °C and is performed in special furnaces with a temperature accuracy of a few degrees [1]. The standards in which artificial aging parameters are recommended are AMS 2772 [2], issued by SAE International Group, and the Aluminum Standard and Data [3], issued by The Aluminum Association.

The common method for the classification of furnaces is by their mode of operation (batch or continuous), by the heating method that they utilize (direct-fired or indirectly heated), and by type of energy that they use (fuel or electricity) [4]. Different manufacturers produce different types of furnaces intending to carry out the aging heat while pursuing the same goals, namely, to ensure improved energy efficiency and provide an environmentally friendly manufacturing footprint. The design of traditional furnaces has been constantly improved along with an important upsurge of the underlying automatic control.

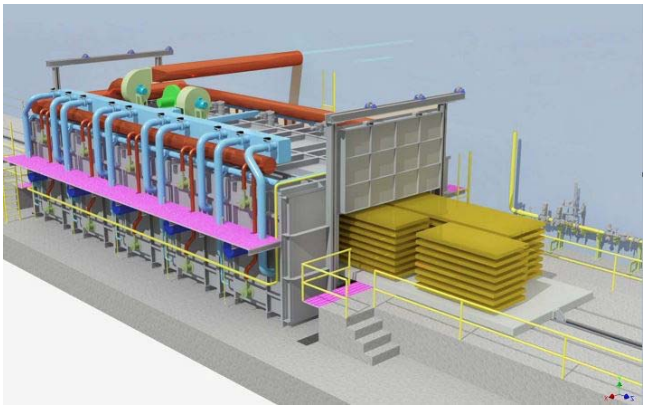

Fig. 1. – Equipment for the aging process of Aluminum alloy sheets.

In all these processes – from the heat treatment to the furnace design – mathematical modeling plays an important role that is sustained by the increase of computing power [5]. This paper is concerned with a mathematical model for a Danieli batch treatment furnace with 70 tons maximum load, indirectly heated, fuel-fired for aluminum alloy plates aging treatment (Fig. 1), which was commissioned in 2019 in the ALRO plant in Romania. The furnace, which is provided with ultimate improvements in temperature control, may safeguard a temperature of ± 3 °C uniformity, within the range of 80 °C – 250 °C, in the workspace.

The models that are known and used in numerical simulations are divided into three main parts: temperature projection, phase conversion, and mechanical performance [6]. In this paper, we focus on the dynamics of the heat transfer and airflow inside the empty and loaded furnace, respectively, from the initial moment up to the steady statue working conditions, when the temperature inside the furnaces reaches a stationary plateau. The steady-state analysis using numerical simulation is reported in [7].

A section of the furnace – the "middle" part – that is defined assuming heat and flow separation, is seen as relevant and forms the basis of this study. Most of the published works on heat and flow concern the loaded furnace and very few works are devoted to the empty furnace, which is the starting point in the heat transfer process analysis. In general, those works that are devoted to empty furnaces regard the treatment of steel [8–10]. Previous studies on the empty furnace for aluminum sheets aging of concern here are presented in [7].

In what follows, the forced convection heat transfer – from the beginning of the process up to the steady-state operation mode – and the internal, underlying turbulent airflow is studied. Tests and measurements are used to compare with and validate the numerical results, including the temperature uniformity survey (TUS) test. Once confidence in the numerical model outputs is gained, diverse scenarios and strategies can be contemplated, *e.g.*, to optimize the aging process by loading the furnace and simulating the variation of the batch volume, the dimensions of the plates, and their position in the furnace.

2. FORCED CONVECTION HEAT TRANSFER

Heat transfer combines all modes: conduction (in all parts), convection (within the airstream), and radiation

[1] Department of Electrical Machines, Materials and Drives, University Politehnica of Bucharest, Splaiul Independenţei 313, 060042, Bucharest, Romania, E-mail: amm@iem.pub.ro, yelda.veli@upb.ro, alin.dobre@upb.ro
[2] Vimetco ALRO, Str. Pitești 116, 230048, Slatina, Romania, E-mail: mapetre@alro.ro

(between corresponding surfaces). Radiation heat transfer may be important in the initial phase of the process and more heating power may be needed to reach the working temperature inside the furnace. We acknowledge this fact, and future work will be devoted to clarifying this aspect.

Air is assumed to be a viscous, Newtonian fluid, and its hydrodynamic and thermal properties are considered constant, evaluated at working temperature and atmospheric pressure. The reason is that, except for the vicinity of burners, the stationary system is almost isothermal. This assumption will be discarded in a future study.

Despite these two restrictive assumptions concerning the radiation heat transfer and the temperature dependence of the properties, as will be seen, the numerical simulation results compare satisfactorily well with the available experimental data although radiation heat transfer is discarded here.

The thermal properties of air are assessed at the bulk, operational temperature of the batch. It is assumed that there is no mixed (natural and forced) to contribute to the convection heat transfer inside the furnace. The hydrodynamic airflow is then assumed stationary – the time to its inset is negligibly small when compared with the thermal inertia and time constants (scales) of the system. The energy balance closes the physical and mathematical model.

A k-ω model [13,14,7], where is k [J/m^3] the kinetic energy of turbulent fluctuations per unit mass and ω [m^2/s^3] is the specific dissipation rate (of vorticity-vector magnitude), presents the momentum conservation

$$\rho(\mathbf{u}\cdot\nabla)\mathbf{u} = \nabla\cdot\left[-p\mathbf{I} + (\eta+\eta_T)\left(\nabla\mathbf{u} + (\nabla\mathbf{u})^{\mathrm{T}}\right) - (2/3)\rho k\,\mathbf{I}\right] - \\ -\nabla\cdot\left[(2/3)(\eta+\eta_T)(\nabla\cdot\mathbf{u})\mathbf{I}\right], \quad (1)$$

to which add:

- *the RANS equation for the turbulence kinetic energy balance*

$$(\rho\mathbf{u}\cdot\nabla)k = P - \beta^*\rho k\omega + \nabla\cdot\left[(\eta+\sigma_k\,\rho k/\omega)\nabla k\right], \quad (2)$$

- *the RANS equation for the specific rate of dissipation of kinetic energy balance*

$$(\rho\mathbf{u}\cdot\nabla)\omega = \frac{\alpha\omega}{k}P - \beta\rho\omega^2 + \nabla\cdot\left[(\eta+\sigma_\omega\,\rho k/\omega)\nabla\omega\right]. \quad (3)$$

Here $\mathbf{u}$ [m/s] is the velocity, p [N/m^2] the pressure, ρ [kg/m^3] the mass density, η [Pas] the dynamic viscosity, $\mathbf{I}$ the unity matrix,

$$P(\mathbf{u}) = (\rho k/\omega)\begin{bmatrix}\nabla\mathbf{u}:\left(\nabla\mathbf{u}+(\nabla\mathbf{u})^{\mathrm{T}}\right) - \\ -(2/3)(\nabla\cdot\mathbf{u})^2\end{bmatrix} - (2/3)\rho k\nabla\cdot\mathbf{u},$$

Ma = $|\mathbf{u}|/a_{air}$ is the Mach number, and a_{air} is the velocity of the sound in the air. The eddy viscosity required by the Reynolds-averaged Navier-Stokes (RANS) equations is η_T. The recommended values for the parameters that intervene above are available in [12].

The k-ω model provides for an approximation of the RANS equations. It introduces two variables: k, the turbulence kinetic energy, and ω, the specific rate of dissipation of kinetic energy (turbulence frequency). As compared with k-ε models [15, 16] – that account for ε, the rate of dissipation of turbulence kinetic energy, instead of ω – that is adequate for external flows about complex geometries, but do not perform satisfactorily inflows driven by large adverse pressure gradients [13], the Wilcox model is recommended for internal flows that exhibit strong curvature, separated flows, and jets.

The mass balance (compressible mode)

$$(\nabla\cdot\rho\mathbf{u}) = 0, \quad (4)$$

closes the hydrodynamic problem.

The energy equation

$$\rho c_p\left[\frac{\partial T}{\partial t} + (\mathbf{u}\cdot\nabla)T\right] = \nabla\cdot(k\nabla T), \quad (5)$$

where k [W/m^{2}K] is the thermal conductivity and c_p [J/kgK] is the specific heat, presents the heat transfer part of the model. The convective term in the left side of Eq. (5) is canceled for the solid parts of the model, and in the regions of airflow, the velocity field is obtained from the hydrodynamic problem.

The boundary conditions that close the mathematical model, depicted in Fig. 2, are as follows:

- *for the airflow* (in blue):
  - inlet speed for the air to enter the fan (10 m/s);
  - no-slip for solid walls;
  - slip condition for vertical symmetry (cut) planes;
- *for heat transfer* (in red):
  - convection heat transfer to the outside and air-heated surfaces, respectively the upper and sidewalls of the furnace.
  - insulation for symmetry (cut) planes;
  - constant temperature (40 °C) or thermal insulation for the bottom of the furnace.

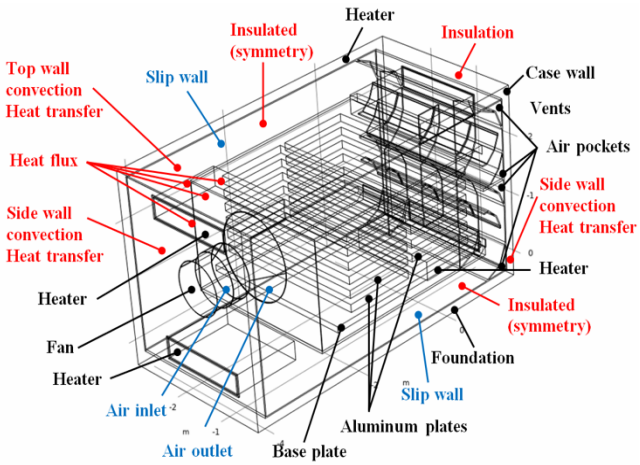

Fig. 2 – Computational domains and boundary conditions. Dimensions are in meters.

For the corner (side) cell, the solid (external) no-slip flow condition is set for the face of the wall washed by the air, and convection heat transfer to the surroundings is set for the face of the wall exposed to the environment.

The initial thermal conditions are those of the hall, *i.e.*, 20 °C. The airflow inside the furnace is in a closed circuit.

3. NUMERICAL SIMULATION CONCERNS

The mathematical model defined by Eqs. (1)–(3) is solved numerically, using the finite element method (FEM).

Figure 3 shows the unstructured FEM mesh for the "middle" cell, which represents the central, modular part of the furnace. The network consists of approx. 1.3 million tetrahedral, quadratic, Lagrange elements, as shown using an automatic mesh generator (Delaunay).

It should be noted that this discretization technique considers the spatial structure, the so-called "geometry", the computational domain, and not the physical problem to be solved – here, heat transfer through thermal conduction, forced convection, and thermal radiation. The quality of the discretization network must be evaluated concerning the physical-mathematical model to be solved.

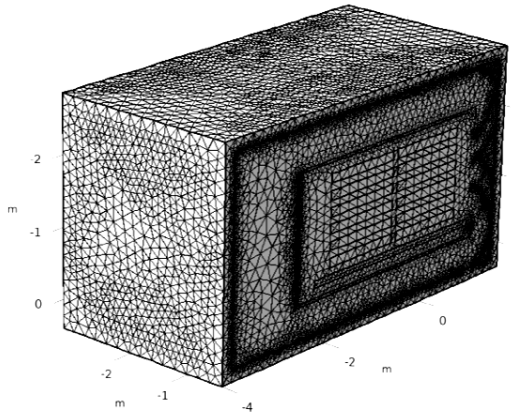

Fig. 3 – The unstructured FEM mesh made of approx. 1,3 mil. of tetrahedral, Lagrange, quadratic elements.

3.1. LOCAL MACH NUMBER, TURBULENT FLOW MODELING – THE COMPRESSIBLE FLOW REGIME

A difficulty that is encountered in mathematical modeling when using asymptotic-like models such as *k*-ω, Eqs. (1)–(3), is that, depending on the local forced flow, parts of the air stream may be either above or below the *local* Ma value, which sets the compressible/incompressible flow threshold, namely Ma < 0.3. This *local* condition is difficult (if possible) to verify.

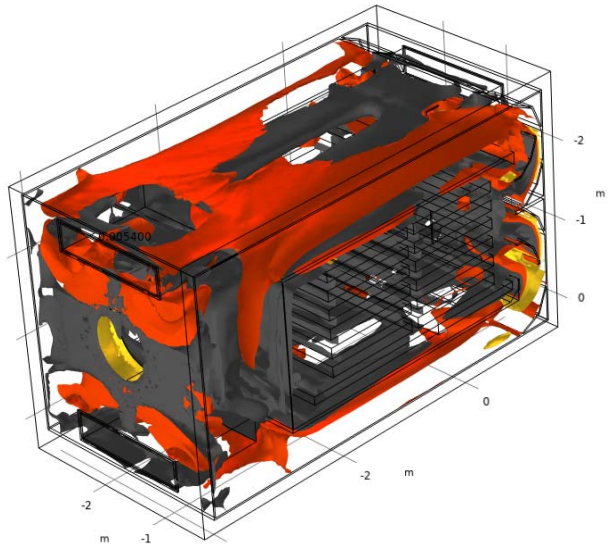

Fig. 4. – Surfaces of constant Ma (red) indicates higher Ma); Ma_{max} = ~0.032 for U_{in} = 15 m/s.

In the absence of a model that may smoothly accommodate the transition between compressible and incompressible flows, we initially assume that the flow regime that is driven by the inlet velocity boundary conditions is compressible. It is then left for an *a posteriori* inspection of the local Ma number that is found based on numerical simulation to learn the validity of this assumption.

Figure 4 presents the local Ma number through iso-surfaces for 15 m/s inlet velocity, higher than 10 m/s used in this study. The Ma < 0.3 conditions are fulfilled, which strengthens the initial compressible flow assumption.

3.2. STABILITY, CONVERGENCE, AND ACCURACY OF NUMERICAL SOLUTIONS FOR THE AIRFLOW AND THE HEAT TRANSFER

In numerical modeling of flow and heat transfer problems based on domain methods, the discretization network must ensure the numerical stability and convergence of the solution. Two of the quality indicators of the numerical grid are the local quantities *cell* Reynolds (Re_{cell}) and *cell* Peclet (Pe_{cell}) numbers. The two numbers are defined using the local speed (at the cell level) and the characteristic size of the cell [*e.g.*, the longest side (edge) of the cell perimeter (surface)]. Re_{cell} is defined as the ratio of inertial to viscous forces and Pe_{cell} is the ratio of convective to diffusive heat fluxes passing through the cell

$$Re_{cell} = UL/\nu, \quad Pe_{cell} = Re_{cell}Pr, \tag{6}$$

where U [m/s] is the local velocity (a reference quantity), L [m] is the local length scale (of the size of the discretization cell, *e.g.*, the finite element), ν [m^2/s] is the kinematic viscosity, Pr = ν/α is Prandtl group, and $\alpha = k/(\rho c_p)$ [m^2/s] is the thermal diffusivity [17]. The "cell" is, in this context, the *local control volume* (*e.g.*, the finite element cell) that is produced by FEM-meshing the computational domain.

In numerical modeling it is recommended for the grid to have the necessary resolution to ensure the "transferability" of physical quantity of concern. For small Re_{cell} and Pe_{cell} numbers the diffusion (conduction) of a property (velocity, respectively temperature) is more important than the convection (transport) of that property inside the cell. Thus, given these indicators, for small Re_{cell} and Pe_{cell} numbers the discretization schemes must have the necessary resolution ("fineness") for the supposed diffusion process to be the principal feature, while for large Re_{cell} and Pe_{cell} the grid must have the necessary resolution so that the presumed convection of the property (physical size, transported field) is the main feature.

The geometric discretization of the computational domain is only the first, very important stage of the numerical modeling process. It is necessary to adjust it further to meet the quality criteria measured with these two local parameters – Re_{cell} and Pe_{cell} numbers. This is where the physical models of concern come into play.

Reynolds cell number criterion, transition to turbulence. Reynolds number (group) is introduced in studies on viscous flows in pipes and channels.

There is a critical Reynolds number (based on the flow size, *e.g.*, the hydraulic diameter), Re_{cr}, above which the flow becomes unstable and turbulent – Reynolds has shown experimentally that this critical threshold is between 11,800

and 14,300. This threshold is overestimated and may be justified using very smooth inlets in the experiments performed. However, many experimental results show that $Re_{cr} \approx 2{,}000$. On the other hand, in other works – especially studies using very smooth pipes [18] – laminar flow has been observed for Re up to 100,000.

If the results of the experiments [19] are correct, it follows that the laminar flow region cannot be limited to Reynolds numbers up to 2,000. The roughness of the wall, the conditions at the entrance to the pipeline can induce instabilities or turbulence, and the flow does not return to the laminar regime if Reynolds group is high enough (> 2,300 for a cylindrical, circular, straight pipe where the length scale is the flow "size", *i.e.*, the hydraulic diameter).

Peclet cell number criterion. The heat treatment plant is a complex system with spaces of all sizes so that there can be both laminar flow regions (*e.g.*, spaces between Al plates) and turbulent flow regions. In these circumstances, the use of a unique mathematical model to characterize the two regimes (laminar and turbulent) and the transitional one is not possible. As a result, establishing a general numerical model valid for the entire computational range (from laminar flow to turbulent flow) is at least difficult (if possible).

The numerical simulation results [7] suggest that, based on Re_{cell}, the flow is turbulent, as presumed.

In this study, we use the Re and Pe cell numbers, currently recommended for laminar flows. For the loaded middle furnace, here, $Re_{cell,max} \sim 9 \cdot 10^3$, and $Pe_{cell,max} \sim 3.4 \cdot 10^4$, consistent with the forced convection in a turbulent flow.

4. NUMERICAL SIMULATION RESULTS

The stationary, compressible, and turbulent airflow – Eqs. (1), (2) – is solved in the first place for the "middle" cell. Figure 5 presents it through arrows and velocity tube lines, whose size and color are proportional to the local flow rate.

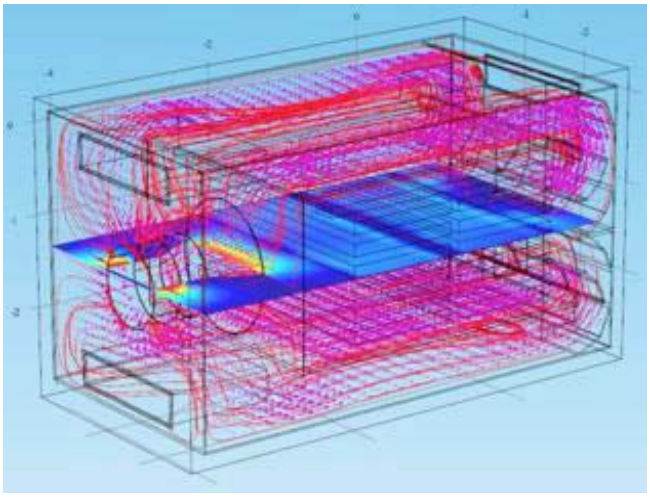

Fig. 5 – The flow field inside the furnace for U_{in} = 10 m/s; U_{max} = 15 m/s.

Once the flow is solved, heat transfer follows. The transient heating mode of the furnace is modeled by adjusting the burners: their power is progressively reduced as the load reaches the nominal temperature. It is assumed that all burners deliver the same thermal power. Figure 6 shows the burner power control diagram that models a temperature-controlled power source.

The control term that is used is defined as

$$P_{control} = P_{burner,stationary} + \\ + \text{switch}(T_{control}, T_{stationary}) \cdot P_{burner,\max} \exp\left(\frac{T_{stationary} - T_{control}}{T_c}\right), \quad (7)$$

where $P_{burner,\ stationary}$ = 700 kW is the stationary thermal power on the module (4 burners), P_{burner} = 20 kW (adjustable) is the initial power per module (4 burners), T_c = 5 min defines the time constant of the thermal control, $T_{control}$ is the temperature measured by the control thermocouple, and switch ($T_{control}$, $T_{stationry}$) = ($T_{control}$ < $T_{stationry}$) is a (Boolean) threshold function. The position of the thermocouple used to adjust $T_{control}$ is shown in Fig. 7.

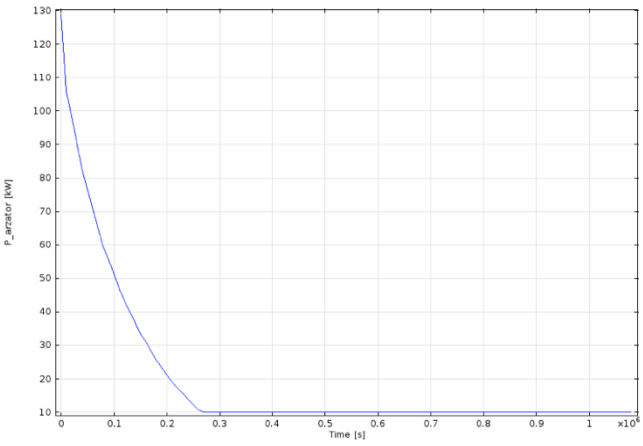

Fig. 6 – Adjusting the power of the burners according to the load temperature measured at the control point (Fig. 9)

These values can be harmonized with the plant-specific working conditions.

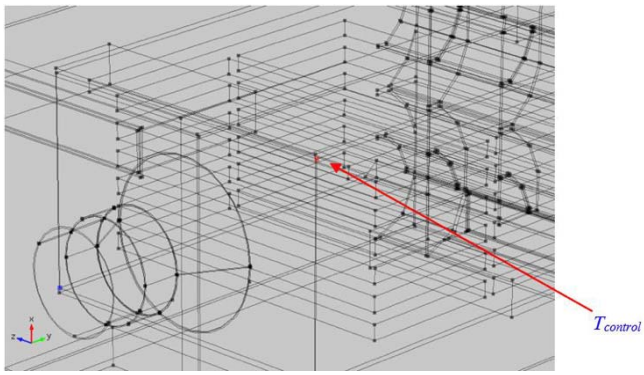

Fig. 7 – The charge temperature monitoring point. The temperature measured here, $T_{control}$, is used to control the power of the burners.

This "threshold" type of control was implemented to enable the reduction of the burner power from the initial value to a steady-state value.

Another approach to the transient heating regime analyzed in this study is to set the level of a permanent operating temperature for burners (their air-bathed surfaces) so that when reaching the stationary regime, after a predetermined duration, the control points of the charge reaches the temperature set in the technological process (*e.g.*, 180 °C in Fig. 10, later).

The experimental charge report for artificial aging is shown in Fig. 8. The temperature excursion in five different reference points, which are used to monitor the accuracy of the aging process on the charge obtained through numerical simulation when using the set level temperature control.

Figure 9 presents the temperature excursion for three different points on the charge until the steady-state aging process is reached (here, approx. 6,5 hours). At this time the initial thermal power of the burners is gradually reduced, as the load reaches the stationary thermal regime, to the limit needed for the process to stay stationary. These results are obtained through numerical simulation when the set level temperature control is used.

For a better approach to the experimental data, the apparent slower temperature upraise seen in the numerical results may be corrected through adjusting $P_{burner,\max}$ and/or the duration of its action, or by changing the location of the station (point) where $T_{control}$ is monitored.

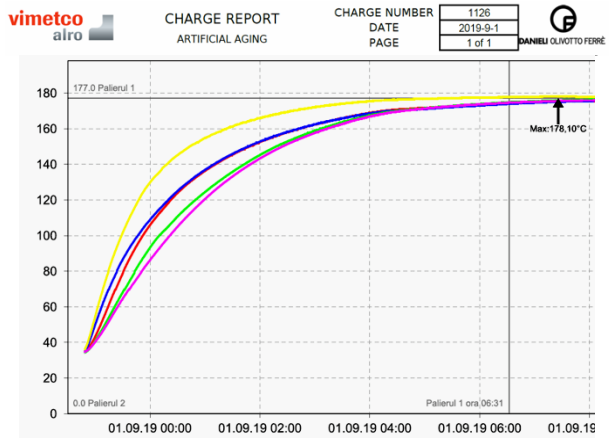

Fig. 8 – The charge temperature report. The time on the abscissa is in hours and the temperature is in deg. C (experimental data).

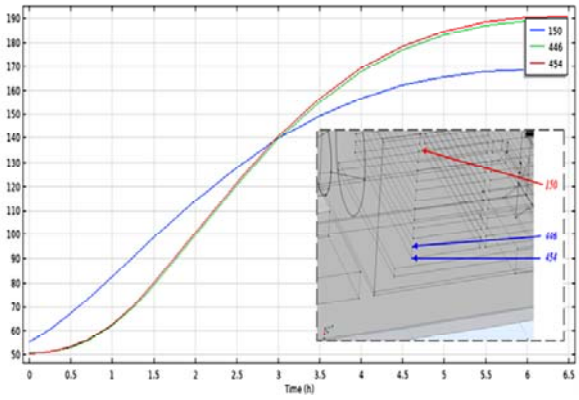

Fig. 9 – Temperature dynamics in three points inside the batch. The temperature is in deg. C (numerical simulation results).

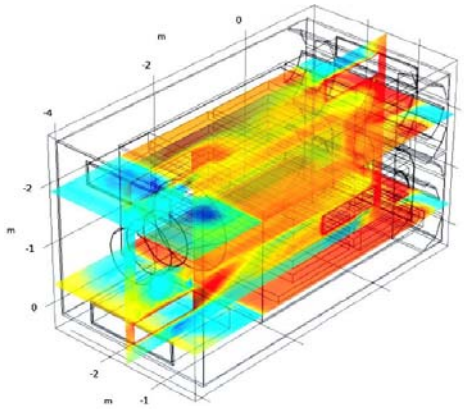

Fig. 10 – The steady state distribution of temperature inside the furnace for U_{in} = 10 m/s. T_{max} ~ 180 °C (red), T_{min} ~ 31°C (blue).

Whereas this convenient power/temperature adjustment may be useful and meaningful in approaching the numerical results to the experimental findings, from a technological point of view the actual temperature control is of concern and relevance. Its implementation may require a hybrid, system/boundary and initial value problem to be formulated and solved. Its implementation is the objective of future research.

The dynamic regime model allows determining the thermal load of the heaters that ensure the treatment of the load further, until reaching the duration of the process – in this case, for the middle module, 4 kW. Figure 10 shows the temperature distribution, practically isothermal, at 180 ° C, in the middle cell.

5. CONCLUSIONS

The main results obtained in this study can be summarized as follows:

The phases of heat treatment of artificial aging up to a certain temperature and maintaining in a defined interval around this temperature a well-defined period can be analyzed by mathematical and numerical modeling, to predetermine the main process parameters.

Mathematical modeling requires the construction of a computational as close as possible to reality, but numerically treatable with a reasonable and accessible horse effort. The CAD models developed for this purpose adequately reproduce the essential features of the analyzed aging equipment. As the size of the installation (complexity) exceeds the resources allocated in this study, symmetry, periodicity, and "separation" conditions were used to build models that can reproduce the hydrodynamic and thermal processes characteristic of the installation.

The airflow regime was assumed to be turbulent (Wilkox model, k-ω) – a hypothesis supported by similar studies and confirmed, here, *a posteriori* by numerical evaluation. The heat transfer problem is of forced convection type, with convective and radiative heat sources – the established limit and initial conditions respect the operating conditions of the installation. From the analysis of the local Mach number, it was found that the analyzed flows verify the hypothesis of compressibility. Moreover, local (cell) Reynolds and Peclet numbers validate the turbulent flow forced convection regime hypothesis.

The dynamic regime analyzed in the hypothesis of an isothermal control at the power of the heaters allows the determination of the thermal power of the stationary regime of the installation. Thus, the presented simulation results obtained for dynamic (starting) and stationary (duration) regimes agree satisfactorily well with the available experimental data.

The study can be continued in the sense of modeling the entire system, as well as predetermining the behavior of the installation in particular regimes.

ACKNOWLEDGEMENTS

Part of the cost of the industrial equipment used to obtain the results presented in this work was funded by European Union through Competitiveness Operational Program, Priority Axis 1 Research, Technological Development, and Innovation, within the project "Investments in the R&D Department of ALRO aiming at improving the research infrastructure for the aluminum alloy heat treated plates with

high qualification industrial applications", based on the Funding Contract no. 42/05.09.2016. Numerical simulations were conducted in the Laboratory for Multiphysics Modeling at the University Politehnica University of Bucharest.

Received on 22 February 2022

REFERENCES

1 A.P. Mouritz, *Introduction to Aerospace Materials, Aluminum Alloys for Aircraft Structures*, Woodhead Publishing, 2012, pp. 173-201.
2 *** ANSI WebStore, SAE AMS 2770J-2011 (SAE AMS2770J-2011), https://webstore.ansi.org/standards/sae/saeams2770j2011ams2770j?gclid=CjwKCAiAsNKQBhAPEiwAB-I5zXhy804OpUmCwaedvUj4fkmX-l-VAEzaTHfZ2yfuItRravloANnSRBoCHy0QAvD_BwE
3 *** Aluminum standard for AAS, *Aluminum standard for AAS*, https://www.sigmaaldrich.com/RO/en/product/sial/06154?gclid=CjwKCAiAsNKQBhAPEiwAB-I5zX8p0J8PT7yu1zjZdcefwlEkRJQCvId6ArbzkKBPzU6yhGQVaYGGaBoCaLMQAvD_BwE
4 M. Belte, D. Dragulin, A.T.C. Aluvation, *Importance of the cooling rate during the heat treatment process of aluminum*, Int. Aluminium J., pp. 61-64, 2018.
5 M. Popa et al., *Coupled fluid flow, and heat transfer analysis of aging heat furnace*, Light Metals 2019, Springer International Publishing.
6 J. Rohde, A. Jeppsson, *Literature review of heat treatment simulations with respect to phase transformation, residual stresses, and distortion*, Scand. J. Metall., **29**, *2*, pp. 47-62, 2010.
7 Y. Veli, M. Petre, A.M. Morega, A.A. Dobre, A.V. Necola, *Finite element method analysis of flow and heat transfer of aging heat furnace for aluminum alloy plates*, INCAS Bull., **14**, *1*, 2022 (in press).
8 J. Mackerle, *Finite element analysis and simulation of quenching and other heat treatment processes: A bibliography (1976–2001)*, Computational Materials Science, **27**, *3*, pp. 313-332, 2003.
9 R. Purushothaman, *Evaluation, and Improvement of Heat Treatment Furnace Model*, PhD Thesis, Worcester Polytechnic Institute, June 2008.
10 E. Hachem, *Stabilized finite element method for heat transfer and turbulent flows inside industrial furnaces*, Mechanics [physics. med-ph]. École Nationale Supérieure des Mines de Paris, PhD Thesis, 2009.
11 D. Saber, H. M. Almalki, Kh. Abd El-Aziz, *Design, and building of an automated heat-treatment system for industrial applications*, Alexandria Engineering J., **59**, *6*, 2020, pp. 5007-5017, 2020.
12 *** *Pyrometry AMS2750F*, *AMS B Finishes Processes and Fluids Committee*, SAE International, 2020-06-29.
13 D. C. Wilcox, *Turbulence Modeling for CFD*, 2nd ed., DCW Industries, 1998.
14 D. C. Wilcox, *Formulation of the k–ω turbulence model revisited*, AIAA J., **46**, pp. 2823-2838, 2008.
15 W. P. Jones, B. E. Launder, *The prediction of laminarization with a two-equation model of turbulence*, International J. of Heat and Mass Transfer, 15, pp. 301-314, 1972.
16 B. E. Launder, B. I. Sharma, *Application of the energy dissipation model of turbulence to the calculation of flow near a spinning disc*, Letters in Heat and Mass Transfer, **1**, *2*, pp. 131-138, 1974.
17 A. Bejan, *Heat Transfer*, Wiley India Edition, 2011.
18 V. Kriventsev, H. Ohshima, A. Yamaguchi, H. Ninokata, *Numerical prediction of secondary flows in complex areas using the concept of local turbulent Reynolds number*, J. of Nuclear Science and Technology, **40**, *9*, pp. 655–663, 2003.
19 W. Pfeninger, *Transition Experiments in the Inlet Length of Tubes at High Reynolds Numbers, Boundary Layer and Flow Control*, ed. G. V. Lachman, Pergamon, pp. 970–980, 1961.